Editors' Suggestion | Featured in Physics

Hydrodynamics-Induced Long-Range Attraction between Plates in Bacterial Suspensions

Luhui Ning,[1,2,3,*] Xin Lou,[2,3,*] Qili Ma,[1] Yaochen Yang,[4,2] Nan Luo,[1,2] Ke Chen,[1,2,5] Fanlong Meng,[4,2,3] Xin Zhou,[2,3] Mingcheng Yang,[1,2,5,†] and Yi Peng[1,2,‡]

[1]*Beijing National Laboratory for Condensed Matter Physics and Laboratory of Soft Matter Physics, Institute of Physics, Chinese Academy of Sciences, Beijing 100190, China*

[2]*School of Physical Sciences, University of Chinese Academy of Sciences, Beijing 100049, China*

[3]*Wenzhou Institute, University of Chinese Academy of Sciences, Wenzhou, Zhejiang 325001, China*

[4]*CAS Key Laboratory for Theoretical Physics, Institute of Theoretical Physics, Chinese Academy of Sciences, Beijing 100190, China*

[5]*Songshan Lake Materials Laboratory, Dongguan, Guangdong 523808, China*

(Received 30 March 2023; accepted 23 August 2023; published 10 October 2023)

We perform optical-tweezers experiments and mesoscale fluid simulations to study the effective interactions between two parallel plates immersed in bacterial suspensions. The plates are found to experience a long-range attraction, which increases linearly with bacterial density and decreases with plate separation. The higher bacterial density and orientation order between plates observed in the experiments imply that the long-range effective attraction mainly arises from the bacterial flow field, instead of the direct bacterium-plate collisions, which is confirmed by the simulations. Furthermore, the hydrodynamic contribution is inversely proportional to the squared interplate separation in the far field. Our findings highlight the importance of hydrodynamics on the effective forces between passive objects in active baths, providing new possibilities to control activity-directed assembly.

DOI: 10.1103/PhysRevLett.131.158301

Introduction.—Interaction forces between mesoscopic particles are crucial for the stability, phase behaviors, and rheology of complex fluids. These interactions have multiple origins, including electrostatic force, van der Waals force, and steric interaction [1]. Particularly, in solutions containing an overwhelming number of smaller background agents, the suspended particles experience an effective depletion force that is independent of microscopic fluid molecules and originates from entropy. Recently, the effective interaction has been generalized to active fluids [2–15], where the agents are self-propelled units, such as bacteria [16–18] and artificial motile colloids [19–21]. The active agents can drastically change the effective interaction between immersed passive objects, giving rise to unusual properties unattainable in thermal baths, such as giant [4,5,12,13], oscillating [3–11,15], long-range [2–4,14], and even constraint-dependent effective forces [10]. Exploiting the effective interaction in active fluids is fundamentally important to design and manipulate activity-directed assembly and transportation.

Until now, most simulation studies on the active effective interactions have been implemented in dry active systems [2–13], where the fluid-mediated hydrodynamic effects are not considered, and the active effective forces are solely attributed to direct collisions between the active agents and passive objects. Nevertheless, surprisingly, the reduced simulations can well reproduce the experimental results of the active effective force between two passive spheres [9,10] and between a circle boundary and a passive disk immersed in active baths [11], implying that the hydrodynamic effects may not be important for the active effective force in these situations. This implication is counterintuitive because the flows generated by active agents significantly influence the self-organized structures and dynamics of both active and passive objects [15,22–28]. Particularly, the hydrodynamic interactions between bacteria and a solid surface largely cause the bacteria to accumulate and swim parallel to the surface [23,29,30]. The seemingly inconsistent observations above thus raise an intriguing question: how does hydrodynamics generally impact the active effective interaction in active fluids?

In this Letter, we study the effective interactions between two plates immersed in bacterial suspensions by combining experiments and fluid simulations. The platelike objects, which are widely used in reduced simulations [2–6], are chosen for two reasons. First, the plates can effectively minimize the interobject concave gap where active particles tend to accumulate [2,4,5], hence weaken the active particle-object collisions. Second, the plates can facilitate the alignment of active particles [24,29,31–36], thus enhance the hydrodynamic contribution. Both experiments and simulations demonstrate the presence of a long-range effective attraction between two plates. Moreover, video microscopy reveals that the bacterial density and alignment with plates are higher inside the gap of the plates than outside. Considering that the direct collisions of the plates with excess bacteria inside the gap should produce an effective repulsion, the obtained long-range effective

attraction between the plates is suggested to originate from the bacterial flow field. The hydrodynamic contribution to the effective force is directly quantified in simulation, which overwhelms the repulsion from direct bacterium-plate collisions, consistent with the experiments.

Experiment.—We employ suspensions of *Escherichia coli* (*E.coli*) as our model active fluids [37]. Our measurement shows that a rodlike bacterium has a length of $l = 3.0 \pm 0.11\ \mu\text{m}$ and a diameter of $\sigma = 1.0 \pm 0.13\ \mu\text{m}$, swimming at $v_E = 10.8 \pm 0.88\ \mu\text{m/s}$ in deionized water. The far-field flow created by a swimming *E.coli* is well described by the extensile dipolar flow [23]. The plates are fabricated lithographically using SU-8 polymer [53], which are $(20.0 \times 7.5 \times 7.5)\ \mu\text{m}^3$ in shape. A dilute dispersion of plates are mixed with bacterial suspensions to get four different volume fractions of bacteria ($\phi = 0.05$, 0.07, 0.10, and 0.13), which is sealed in a closed chamber to avoid chemotaxis and external flows [37]. A few polystyrene (PS) beads with diameter of $\sigma_p = 10.0\ \mu\text{m}$ are used as spacers to keep the sample thickness at 10.0 μm. The images are recorded by bright-field microscope (Nikon Ti-U) with a water-immersed 60× objective lens and a camera at 30 frames/s. The positions of the plates and bacteria are extracted using customized particle tracking techniques [41].

The two plates are held parallel in the bacterial suspension by optical tweezers (Aresis Tweez 250si) on the focal plane of the microscope [Fig. 1(a)], which is roughly positioned at the middle of the samples in the z direction, ensuring that the plates do not touch the chamber surfaces [37]. To prevent the plates from turning over during experiments, eight optical traps are employed to hold each plate [37]. The bacterial motion and number density distribution are not affected by the irradiation of optical tweezers due to the negligible laser intensity outside the region occupied by the plates [37]. The two plates fluctuate slightly around the centers of optical traps with an instantaneous face-to-face separation d from each other. Immersed in water without bacteria, each plate experiences no net force and thus zero effective interaction with the other plate with a mean separation d_f. Subsequently, d_f is used as the baseline for zero effective force. Under the same setting of optical traps, the mean separation of two plates in bacterial suspensions differs from the equilibrium state (without bacteria), resulting in a mean deviation $\langle \Delta d \rangle = \langle d \rangle - d_f$. Using $\langle \Delta d \rangle$ and the effective stiffness k of optical traps, which can be determined from the position distribution of trapped plates immersed in bacteria-free water [37], we can obtain the effective force, $F_{\text{eff}} = [(-k\langle \Delta d \rangle)/2]$, for each plate. We record the positions of the plates immersed in bacterial suspensions for 4 min in a single measurement. For each separation and bacterial concentration, 4–16 independent measurements have been performed to obtain $\langle \Delta d \rangle$.

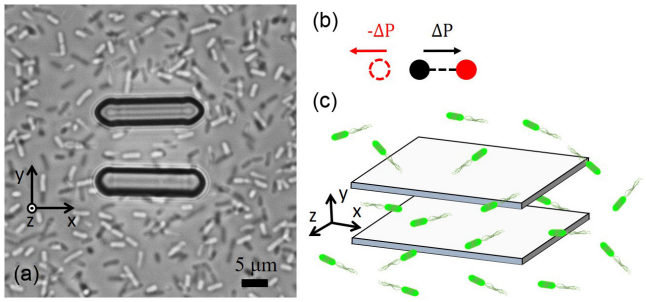

FIG. 1. (a) Snapshot of two plates trapped by optical tweezers in the bacterial suspension. The particles with black edges are the plates, and the small rodlike particles are bacteria. Scale bar: 5 μm. (b) In simulation, the bacterium is modeled as a dimer connected by two beads via a rigid spring. Here, an impulse ΔP is imposed on the dimer, meanwhile, an opposite impulse is applied on fluid elements in the red circle during the dimer moving. (c) Schematic of two parallel plates fixed in the bacterial solution in simulation.

Simulation.—To bridge the length and timescales between *E.coli* and fluid particles, we employ a hybrid mesoscopic scheme to simulate the bacterial suspension containing two fixed parallel plates. The fluid is described by multiparticle collision dynamics (MPC) [54–57], which properly capture hydrodynamic effects and thermal fluctuations, while bacteria are simulated using molecular dynamics (MD). In MPC, the fluid is modeled by a collection of point particles with mass m, whose dynamics evolves by alternating streaming and coarse-grained collision steps. In the collision step, the particles are sorted into square collision cells with a size of l_c. In MD, the *E.coli* is modeled as a rigid dimer composed of two connected beads with a diameter of $\sigma = 2$ [37]. Different *E.coli* interact through their constituent beads via a repulsive Lennard-Jones type potential, $U(r) = 4[(\sigma/r)^{48} - (\sigma/r)^{24} + \frac{1}{4}]$, $r \leq 2^{(1/24)}\sigma$. The bacterial beads couple with the fluid particles via the MPC collisions. By applying an impulse ΔP to the dimer at each MPC step, the bacterium can swim along its orientation vector with a Péclet number comparable to that in experiments [37]. Simultaneously, an opposite ΔP is exerted on a fluid element behind the dimer to locally conserve momentum [Fig. 1(b)], creating a phantom flagellum [48]. This driving operation leads to a pusherlike flow field around the dimer [37]. Three different bacterial volume fractions ($\phi = 0.06$, 0.08, 0.11) are studied here. During the simulation, all the units are dimensionless by setting $l_c = 1$, $m = 1$, and the thermal energy $k_B T = 1$.

The plate is modeled as a cuboid with dimensions of 20 in length, 7.5 in width, and 1.0 in thickness. The two parallel plates are fixed in the middle of the system (with dimensions of $40 \times 100 \times 40$), with the separation d_f, as sketched in Fig. 1(c). The interactions between bacterial beads and plates are described by the repulsive potential mentioned above, while the plates are coupled with the fluid by the no-slip boundary, realized by the bounce-back

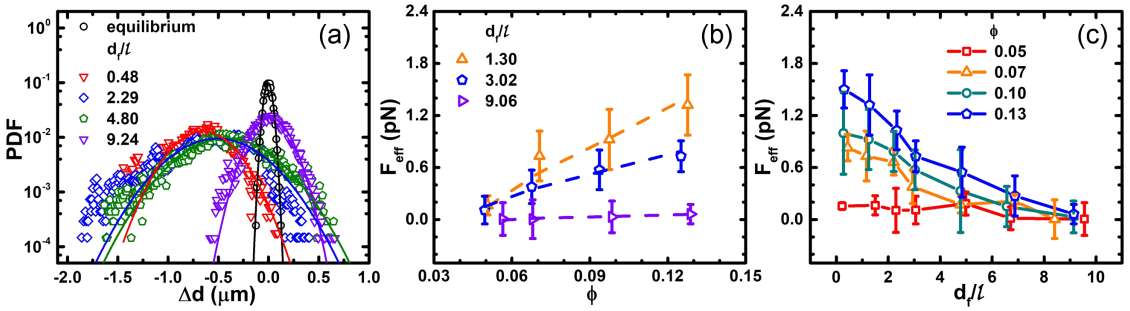

FIG. 2. (a) The PDFs of deviation Δd for $d_f/l = 4.80$ without *E.coli* and for four different d_f/l at $\phi = 0.13$. The solid lines are Gaussian fits. (b) The relation between the effective force F_{eff} and ϕ at different d_f/l. A positive F_{eff} represents an attractive force between two plates. (c) F_{eff} as a function of d_f/l at different ϕ. The symbols and error bars represent the mean and standard deviation calculated over 4–16 independent measurements, respectively.

collisions. In the simulation, the effective forces on the plates contributed by the fluid and bacterium-plate collisions can be separately quantified. See [37] for more simulation details.

Result and discussion.—We first measure the effective force of the two plates immersed in bacterial suspensions. Figure 2(a) shows the probability distribution functions (PDFs) of the instantaneous deviation Δd from the mean separation d_f of the plates. In the absence of bacteria, the PDF follows a Gaussian distribution [37]. However, in the presence of bacteria, the PDF becomes asymmetric at small d_f, with the peak shifting towards smaller separations and the coefficient of skewness $\gamma_1 < 0$, indicating an effective attraction between the plates. The asymmetry of the distribution decreases with d_f and vanishes ($\gamma_1 \approx 0$) at a large separation ($d_f/l = 9.24$) [37]. From $\langle \Delta d \rangle$ and k, we calculate the effective force [Figs. 2(b) and 2(c)]. The effective interaction is purely attractive for all considered ϕ and d_f. Specifically, the attraction increases linearly with ϕ when the separation d_f remains fixed, due to the fact that the Stokes flow generated by swimming bacteria at low Reynolds number is proportional to ϕ [24,43] for all concentrations studied where bacterial collective swimming is absent [37]. Conversely, when ϕ is fixed, the force decreases monotonically with the separation. At the high concentration ($\phi = 0.13$), the attraction remains nonzero even when $d_f/l = 7.0$ ($d_f = 21$ μm).

To better understand the microscopic origins of the long-range effective attraction, we investigate the spatial density distributions and orientation order of bacteria surrounding two trapped plates. The local density and orientation order are measured within a series of rectangular bins (10×4.6 μm^2) parallel to the plate at various positions along the y axis, Y, covering the region around the plates. The local orientational order is defined as $Q = \langle |\cos\theta| \rangle$, where θ represents the angle of a bacterial body relative to the plate and $\langle\rangle$ denotes the ensemble average. $|\cos\theta|$ can be mapped one-to-one to $\cos 2\theta$, characterizing the nematic order of bacterial bodies. The relative density ρ_r, which is the ratio of the local density to bulk density, and Q are shown in Figs. 3(a)–3(d) as a function of Y for four different d_f. For all d_f/l, the bacterial concentration and orientational order near the plates are significantly larger than those in the bulk, indicating that bacteria tend to accumulate near the plates and swim parallel to them. At a small separation ($d_f/l = 0.48$), the number density within the gap between two plates is 3 times of the bulk density, and twice the density near the outer surfaces of the plates. Meanwhile, the bacterial orientational order inside the gap (0.95) is significantly higher than outside (0.82 near the plates and 0.64 in bulk). As d_f increases, the differences in both ρ_r and Q between inside and outside the gap decrease. At $d_f/l = 4.80$, where the effective attraction is 0.6 pN [Fig. 2(c)], the density inside the gap is similar to outside, whereas Q inside the gap is still higher. When the attraction

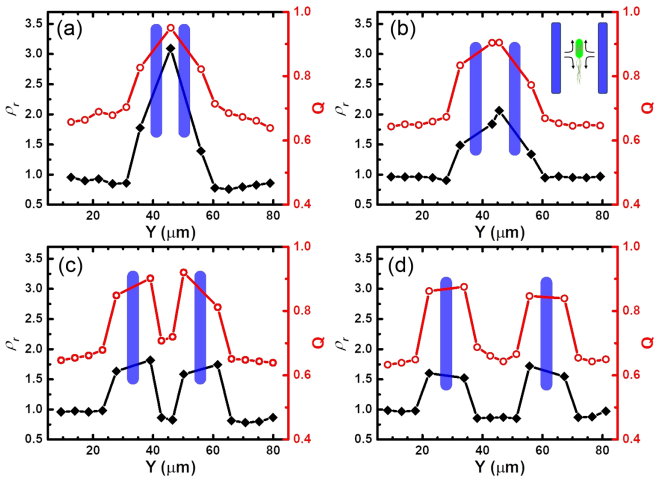

FIG. 3. The distributions of bacterial ρ_r and Q around two plates at four different separations of (a) $d_f/l = 0.48$, (b) 2.29, (c) 4.80, and (d) 8.60. The solid black diamonds and hollow red circles represent the bacterial ρ_r and Q, respectively. The positions of plates are indicated by blue shaded regions. Inset of (b): Sketch of bacterium-induced hydrodynamic attraction between two plates.

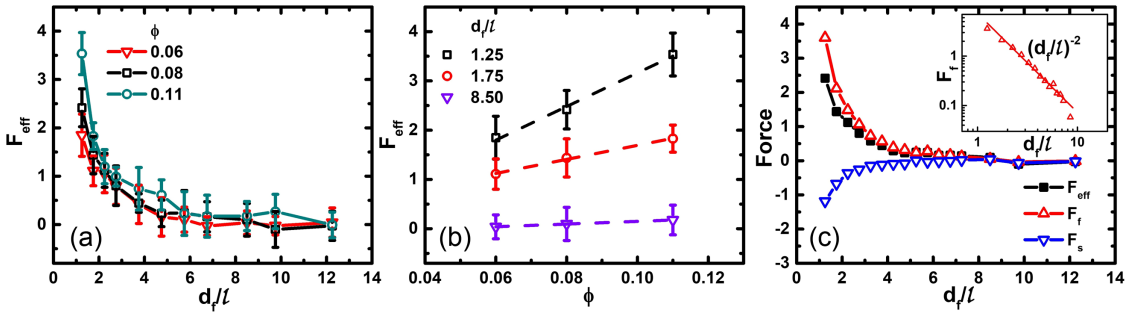

FIG. 4. Simulation results: (a) The effective force F_{eff} as a function of d_f/l for different bacterial concentration ϕ. (b) The relation between F_{eff} and ϕ at different d_f/l. (c) The contributions of the bacterial flow field and direct bacterium-plate collisions to F_{eff} as a function of d_f/l at $\phi = 0.08$. Inset: The red solid line represents a power-law fit.

vanishes at $d_f/l = 9.06$, the ρ_r and Q both become the same inside and outside the gap. Our measurements reveal that the *E.coli* inside and outside the gap exhibit similar swimming speed, $\sim 10.8 \pm 0.88$ μm/s [37].

Our results essentially differ from previous simulations on active depletion forces of platelike objects immersed in dry active baths [2,4–6]. In those studies, a purely effective attraction is also observed in the dilute regime, but accompanying with a lower density of active particles within the gap between plates. This depletionlike attraction, however, exclusively arises from the excess collisions of the plates with their outside active particles, without accounting for hydrodynamic interactions. Additionally, our findings qualitatively differ from the experimental studies on effective interaction between objects with curved surfaces in active colloidal solutions [10,11], where effective repulsion with an oscillating magnitude, rather than effective attraction, is found. This effective repulsion is due to the active particles greatly accumulating into the concave gap formed by the two curved surfaces, and causing intense particle-object collisions inside the concave region. In contrast, the interplate effective attraction in our experiments does not mainly originate from the direct bacterium-plate collisions, since, otherwise, higher bacterial density within the gap between two plates would lead to effective repulsion. Moreover, the larger Q (hence stronger local flow field) between the plates suggests that the hydrodynamics could be a dominant contribution to the effective attraction.

In order to quantify the contributions of hydrodynamic interactions and direct collisions to the effective force, we perform hybrid dynamics simulations, in which the forces from direct bacterium-plate collisions F_s and the flow field F_f can be calculated separately [37]. Figure 4(a) plots the relations between the effective force F_{eff} and separation at different ϕ, where the symbols and error bars, respectively, represent the mean and standard deviation obtained from eight independent simulation runs. The relation between F_{eff} and ϕ is shown in Fig. 4(b). F_{eff} decreases monotonically with d_f/l and increase linearly with ϕ, consistent with our experimental results. Further, we find that F_s and F_f separately produce effective repulsion and attraction [Fig. 4(c)], whose magnitudes monotonically decrease with separation. Interestingly, we found that F_f is always stronger than F_s, resulting in a net effective attraction on the plate. These findings well confirm our above speculation obtained on the base of the experimental observations. Furthermore, F_f decays as $F_f \sim (d_f/l)^{-2}$ [the inset of Fig. 4(c)], reflecting the force dipole nature of bacterial flow field [23]. The forces in simulations [Figs. 4(a) and 4(b)] are dimensionless, so they cannot be directly quantitatively compared with experimental forces. However, by properly mapping the coarse-grained simulation onto a real physical system, the simulation results agree with the experimental ones [37].

The fluid-induced effective attraction can be understood as follows. The flow field generated by a swimming *E.coli* is approximately an extensile force dipole in far field, in which the ambient fluid flows outwards from bacterial head and tail and is compensated by an inward flow towards the waist (side) of the bacterium [23]. Bacteria swimming inside the gap of plates align better with the plates (higher Q) than outside, such that the stronger inward flows towards the bacterial waist inside the gap lead to a hydrodynamic attraction between the surrounding plates [37], as sketched in the inset of Fig. 3(b). The fluid-mediated interaction can be estimated by considering an excess *E.coli* swimming parallel to the plates in the middle of the gap, which is considered as a force dipole. For simplicity, we calculate the force on a slender ellipsoid located $d_f/2$ away from *E.coli*, yielding $F_f \sim (d_f/l)^{-2}$, consistent with the simulation results in the leading order [37]. The simplified model allows us to estimate the effect of top and bottom chamber boundaries on the hydrodynamics-induced attraction. The confinement formed by the chamber boundaries causes F_f decay faster than $(d_f/l)^{-2}$ when d_f is significantly larger than the chamber thickness because the dipolar flow is modified by the no-slip boundaries [49]. The scaling relation, $F_f \sim (d_f/l)^{-2}$, is also observed in experiments when the plate separation

$d_f/l > 3.33$ [37], as the dipolar flow approximation is only valid in far field, i.e., > 5 μm away from a bacterial body [23].

Finally, we emphasize that the competition between direct collision and hydrodynamic interaction depends on the surface shape of the passive objects. The hydrodynamic interaction dominates in the presence of two parallel plates because bacteria align with plate surfaces and high nematic order of bacterial orientation amplifies the hydrodynamic contribution. In contrast, direct collision plays a major role in the experiments of spherical and disklike objects [10,11], in which the concave gap gathers more active particles and hence experiences more collisions from the inside active particles.

Conclusion.—Using experiments and simulations, we show that the effective force between two parallel plates in active bacterial bath exhibits a long-range attraction, which originates from the bacterium-induced fluid flow that overwhelms the repulsive effect caused by direct bacterium-plate collisions. Quantitatively, the hydrodynamics-induced attraction increases linearly with ϕ and decreases with separations as $(d_f/l)^{-2}$, when the force-dipole approximation is valid. These findings have significantly advanced our understanding of effective interaction between passive objects in active fluids, and revealed the fundamental importance of fluid-mediated hydrodynamic effects that have not been adequately considered in previous studies. Furthermore, the competition between hydrodynamic effects and direct collisions from active agents opens a new avenue to control activity-induced effective interactions, which are critical for activity-directed assembly, phase transitions, and transport. Our results are obtained for pusher-type bacteria, so an interesting open question is how important the hydrodynamic contribution is in the cases of neutral and puller-type microswimmers, whose flow fields are a source dipole and a contractile force dipole, respectively.

We acknowledges support from National Natural Science Foundation of China (Grants No. 12074406, No. T2221001, No. 12274448, No. T2325027, No. 12304245) and the Strategic Priority Research Program of the Chinese Academy of Sciences (No. XDB33000000). This work was also supported by the China Postdoctoral Science Foundation (No. 2022M723116).

*These authors contributed equally to this work.
†mcyang@iphy.ac.cn
‡pengy@iphy.ac.cn

[1] J. N. Israelachvili, *Intermolecular and Surface Forces* (Academic Press, New York, 2011).
[2] A. Duzgun and J. V. Selinger, Phys. Rev. E **97**, 032606 (2018).
[3] L. Caprini and U. M. B. Marconi, Soft Matter **14**, 9044 (2018).
[4] R. Ni, M. A. Cohen Stuart, and P. G. Bolhuis, Phys. Rev. Lett. **114**, 018302 (2015).
[5] J. Harder, S. A. Mallory, C. Tung, C. Valeriani, and A. Cacciuto, J. Chem. Phys. **141**, 194901 (2014).
[6] D. Ray, C. Reichhardt, and C. J. O. Reichhardt, Phys. Rev. E **90**, 013019 (2014).
[7] F. Feng, T. Lei, and N. Zhao, Phys. Rev. E **103**, 022604 (2021).
[8] M. Zaeifi Yamchi and A. Naji, J. Chem. Phys. **147**, 194901 (2017).
[9] L. Angelani, C. Maggi, M. L. Bernardini, A. Rizzo, and R. Di Leonardo, Phys. Rev. Lett. **107**, 138302 (2011).
[10] P. Liu, S. Ye, F. Ye, K. Chen, and M. Yang, Phys. Rev. Lett. **124**, 158001 (2020).
[11] S. Paul, A. Jayaram, N. Narinder, T. Speck, and C. Bechinger, Phys. Rev. Lett. **129**, 058001 (2022).
[12] L. R. Leite, D. Lucena, F. Q. Potiguar, and W. P. Ferreira, Phys. Rev. E **94**, 062602 (2016).
[13] S. Gokhale, J. Li, A. Solon, J. Gore, and N. Fakhri, Phys. Rev. E **105**, 054605 (2022).
[14] Y. Baek, A. P. Solon, X. Xu, N. Nikola, and Y. Kafri, Phys. Rev. Lett. **120**, 058002 (2018).
[15] R. C. Krafnick and A. E. García, Phys. Rev. E **91**, 022308 (2015).
[16] J. Tailleur and M. E. Cates, Phys. Rev. Lett. **100**, 218103 (2008).
[17] F. Peruani, J. Starruß, V. Jakovljevic, L. Søgaard-Andersen, A. Deutsch, and M. Bär, Phys. Rev. Lett. **108**, 098102 (2012).
[18] H. Wioland, F. G. Woodhouse, J. Dunkel, J. O. Kessler, and R. E. Goldstein, Phys. Rev. Lett. **110**, 268102 (2013).
[19] I. Theurkauff, C. Cottin-Bizonne, J. Palacci, C. Ybert, and L. Bocquet, Phys. Rev. Lett. **108**, 268303 (2012).
[20] I. Buttinoni, J. Bialké, F. Kümmel, H. Löwen, C. Bechinger, and T. Speck, Phys. Rev. Lett. **110**, 238301 (2013).
[21] J. Palacci, S. Sacanna, A. P. Steinberg, D. J. Pine, and P. M. Chaikin, Science **339**, 936 (2013).
[22] C. Bechinger, R. Di Leonardo, H. Löwen, C. Reichhardt, G. Volpe, and G. Volpe, Rev. Mod. Phys. **88**, 045006 (2016).
[23] K. Drescher, J. Dunkel, L. H. Cisneros, S. Ganguly, and R. E. Goldstein, Proc. Natl. Acad. Sci. U.S.A. **108**, 10940 (2011).
[24] E. Lauga and T. R. Powers, Rep. Prog. Phys. **72**, 096601 (2009).
[25] B. Zhang, P. Leishangthem, Y. Ding, and X. Xu, Proc. Natl. Acad. Sci. U.S.A. **118**, e2100145118 (2021).
[26] X.-L. Wu and A. Libchaber, Phys. Rev. Lett. **84**, 3017 (2000).
[27] Y. Peng, L. Lai, Y.-S. Tai, K. Zhang, X. Xu, and X. Cheng, Phys. Rev. Lett. **116**, 068303 (2016).
[28] P. T. Underhill, J. P. Hernandez-Ortiz, and M. D. Graham, Phys. Rev. Lett. **100**, 248101 (2008).
[29] A. P. Berke, L. Turner, H. C. Berg, and E. Lauga, Phys. Rev. Lett. **101**, 038102 (2008).
[30] S. E. Spagnolie and E. Lauga, J. Fluid Mech. **700**, 105 (2012).
[31] P. Sartori, E. Chiarello, G. Jayaswal, M. Pierno, G. Mistura, P. Brun, A. Tiribocchi, and E. Orlandini, Phys. Rev. E **97**, 022610 (2018).
[32] K.-T. Wu, Y.-T. Hsiao, and W.-Y. Woon, Phys. Rev. E **98**, 052407 (2018).

[33] M. Molaei, M. Barry, R. Stocker, and J. Sheng, Phys. Rev. Lett. **113**, 068103 (2014).
[34] I. S. Aranson, Rep. Prog. Phys. **85**, 076601 (2022).
[35] S. Bianchi, F. Saglimbeni, and R. Di Leonardo, Phys. Rev. X **7**, 011010 (2017).
[36] S. Bianchi, F. Saglimbeni, G. Frangipane, D. Dell'Arciprete, and R. Di Leonardo, Soft Matter **15**, 3397 (2019).
[37] See Supplemental Material at http://link.aps.org/supplemental/10.1103/PhysRevLett.131.158301 for additional experimental, simulation, and theory details, which includes Refs. [9,23,38–52].
[38] J. M. Walter, D. Greenfield, C. Bustamante, and J. Liphardt, Proc. Natl. Acad. Sci. U.S.A. **104**, 2408 (2007).
[39] Y. Peng, Z. Liu, and X. Cheng, Sci. Adv. **7**, eabd1240 (2021).
[40] H.-P. Zhang, A. Beer, E.-L. Florin, and H. L. Swinney, Proc. Natl. Acad. Sci. U.S.A. **107**, 13626 (2010).
[41] Z. Zheng and Y. Han, J. Chem. Phys. **133**, 124509 (2010).
[42] H. Löwen, Phys. Rev. E **50**, 1232 (1994).
[43] J. Elgeti, R. G. Winkler, and G. Gompper, Rep. Prog. Phys. **78**, 056601 (2015).
[44] J. T. Padding and A. A. Louis, Phys. Rev. E **74**, 031402 (2006).
[45] R. Mok, J. Dunkel, and V. Kantsler, Phys. Rev. E **99**, 052607 (2019).
[46] D. Dorić, E. Nikolić-Dorić, V. Jevremović, and J. Malivsić, Qual. Quant. **43**, 481 (2009).
[47] D. P. Doane and L. E. Seward, J. Stat. Educ. **19** (2011).
[48] A. Furukawa, D. Marenduzzo, and M. E. Cates, Phys. Rev. E **90**, 022303 (2014).
[49] S. Ishida, Y. Yang, F. Meng, and D. Matsunaga, Phys. Fluids **34**, 063309 (2022).
[50] J. Hu, M. Yang, G. Gompper, and R. G. Winkler, Soft Matter **11**, 7867 (2015).
[51] J. Happel and H. Brenner, *Low Reynolds Number Hydrodynamics* (Kluwer, Dordrecht, 1991).
[52] Y. Han, A. Alsayed, M. Nobili, and A. G. Yodh, Phys. Rev. E **80**, 011403 (2009).
[53] C. J. Hernandez and T. G. Mason, J. Phys. Chem. C **111**, 4477 (2007).
[54] A. Malevanets and R. Kapral, J. Chem. Phys. **110**, 8605 (1999).
[55] J. T. Padding and A. A. Louis, Phys. Rev. E **74**, 031402 (2006).
[56] R. Kapral, Adv. Chem. Phys. **140**, 89 (2008).
[57] G. Gompper, T. Ihle, D. M. Kroll, and R. G. Winkler, Adv. Polym. Sci. **221**, 1 (2009).